CRISPR/Cas9–Mediated *Tspo* Gene Mutations Lead to Reduced Mitochondrial Membrane Potential and Steroid Formation in MA-10 Mouse Tumor Leydig Cells

Jinjiang Fan,[1] Kevin Wang,[1] Barry Zirkin,[2] and Vassilios Papadopoulos[1,3]

[1]Research Institute of the McGill University Health Centre and Department of Medicine, Faculty of Medicine, McGill University, Montreal, Quebec H4A 3J1, Canada; [2]Department of Biochemistry and Molecular Biology, Johns Hopkins Bloomberg School of Public Health, Baltimore, Maryland 21205; and [3]Department of Pharmacology and Pharmaceutical Sciences, School of Pharmacy, University of Southern California, Los Angeles, California 90089

The outer mitochondrial membrane translocator protein (TSPO) binds cholesterol with high affinity and is involved in mediating its delivery into mitochondria, the rate-limiting step in hormone-induced steroidogenesis. Specific ligand binding to TSPO has been shown to initiate steroid formation. However, recent studies of the genetic deletion of *Tspo* have provided conflicting results. Here, we address and extend previous studies by examining the effects of *Tspo*-specific mutations on steroid formation in hormone- and cyclic adenosine monophosphate (cAMP)–responsive MA-10 cells, using the CRISPR/Cas9 system. Two mutant subcell lines, nG1 and G2G, each carrying a *Tspo* exon2-specific genome modification, and two control subcell lines, G1 and HH, each carrying a wild-type *Tspo,* were produced. In response to dibutyryl cAMP, the nG1 and G2G cells produced progesterone at levels significantly lower than those produced by the corresponding control cells G1 and HH. Neutral lipid homeostasis, which provides free cholesterol for steroid biosynthesis, was altered significantly in the *Tspo* mutant cells. Interestingly, the mitochondrial membrane potential ($\Delta\Psi_m$) of the *Tspo* mutant cells was significantly reduced compared with that of the control cells, likely because of TSPO interactions with the voltage-dependent anion channel and tubulin at the outer mitochondrial membrane. Steroidogenic acute regulatory protein (STAR) expression was induced in nG1 cells, suggesting that reduced TSPO affected STAR synthesis and/or processing. Taken together, these results provide further evidence for the critical role of TSPO in steroid biosynthesis and suggest that it may function at least in part *via* its regulation of $\Delta\Psi_m$ and effects on STAR. **(*Endocrinology* 159: 1130–1146, 2018)**

Steroid hormone biosynthesis begins with the conversion of cholesterol to pregnenolone by the mitochondrial enzyme CYP11A1. This reaction is dependent in part upon delivery of cholesterol from intracellular stores into mitochondria, the latter constituting the rate-determining step in steroidogenesis. Transport of free cholesterol to mitochondria for steroid biosynthesis involves steroidogenic acute regulatory protein (STAR or STARD1), soluble *N*-ethylmaleimide–sensitive factor attachment protein receptor proteins, and interactions of lipid droplets (LDs) with mitochondria and of mitochondria with the endoplasmic reticulum (1–7). STAR and soluble *N*-ethylmaleimide–sensitive factor attachment protein receptor proteins were shown to function

ISSN Online 1945-7170

Received 24 October 2017. Accepted 21 December 2017.
First Published Online 28 December 2017

Abbreviations: Ab, antibody; cAMP, cyclic adenosine monophosphate; cKO, conditional knockout; dbcAMP, dibutyryl–cyclic adenosine monophosphate; DMSO, dimethyl sulfoxide; Ex/Em, excitation/emission; FACS, fluorescence-activated cell sorting; FCCP, carbonyl cyanide 4-(trifluoromethoxy)phenylhydrazone; gRNA, guide RNA; IMM, inner mitochondrial membrane; LD, lipid droplet; Mito-roGFP, mitochondrial reduction-oxidation sensitive green fluorescent protein 1; OFP, orange fluorescent protein; OMM, outer mitochondrial membrane; PBS, phosphate-buffered saline; PKA, cyclic adenosine monophosphate–dependent protein kinase; Q, quarter; STAR, steroidogenic acute regulatory protein; TEM, transmission electron microscopy; TMRE, tetramethylrhodamine ethyl ester; TSPO, translocator protein; VDAC, voltage-dependent anion channel; WT, wild-type; $\Delta\Psi_m$, mitochondrial membrane potential.

primarily outside the mitochondria, where they are considered to be involved in trafficking of free cholesterol to the outer mitochondrial membrane (OMM) (8, 9). This pool of cholesterol must be segregated from the structural cholesterol of OMM and subsequently crosses from the OMM to the inner mitochondrial membrane (IMM) where CYP11A1 is located.

Translocator protein (TSPO; 18 kDa) is a well-conserved, ubiquitous, integral OMM protein that is abundant in steroid-synthesizing cells. With its high affinity for cholesterol, TSPO is able to segregate cholesterol and to participate in its targeting to CYP11A1 (10, 11). Cholesterol binds at a specific binding site of TSPO, the latter termed the cholesterol recognition/interaction amino acid consensus motif (12–14). TSPO-mediated cholesterol targeting to CYP11A1 is likely achieved through the formation of a multiprotein complex of OMM and IMM proteins, including TSPO, voltage-dependent anion channel (VDAC), adenosine triphosphatase family AAA domain–containing protein 3, and CYP11A1 (11). TSPO binds with high affinity to diverse compounds and endogenous ligands that can regulate its activity (5). Biochemical and pharmacological studies using TSPO ligands strongly support the contention that TSPO plays an important role in cholesterol import into mitochondria and thus in steroidogenesis (5, 15, 16). TSPO abundance in steroidogenic cells may be linked to the tissue/cell-specific need for the amounts of free cholesterol to be imported into mitochondria. The presence of TSPO and cholesterol in the OMM may affect mitochondrial membrane fluidity/permeability, fission/fusion processes, membrane protein/transporter function(s), and membrane potential ($\Delta\Psi_m$) (17–19).

Recent studies of genetic deletion of *Tspo* in mice have provided conflicting data, including no effect on steroid synthesis, ablation of corticosteroid response to adrenocorticotropic hormone, and changes in lipid homeostasis in testicular Leydig cells (20–23). Conflicting data based on MA-10 mouse Leydig cells also have been published. Thus, knockdown of *Tspo* expression using antisense oligonucleotides was reported to reduce the ability of the cells to form steroids, but CRISPR/Cas9–guided *Tspo* deletion was reported to have no effect on steroid synthesis (24–26).

The current studies were designed to reevaluate the effect of CRISPR/Cas9–guided *Tspo* deletion on the ability of MA-10 cells to form steroids and to further our understanding of how TSPO functions in this process. TSPO deficiency led to reduced dibutyryl–cyclic adenosine monophosphate (dbcAMP)–stimulated steroid biosynthesis and increased esterified, cholesterol-enriched neutral lipid accumulation, suggesting reduction in the import of the steroidogenic pool of cholesterol into mitochondria. Data suggest that this is most likely due to TSPO-mediated reduced mitochondrial $\Delta\Psi_m$ *via* regulation of VDAC1/tubulin interaction. In addition, we show that STAR levels were increased in TSPO-deficient cells, suggesting that increased STAR expression levels and/or altered STAR processing might compensate to some extent for reduced TSPO. These results support the contention that TSPO plays a major role in steroid biosynthesis and further suggest that TSPO may function at least in part *via* regulation of $\Delta\Psi_m$ and effects on STAR.

Materials and Methods

Cell culture

MA-10 cells were maintained in Dulbecco's modified Eagle medium/F-12 medium supplemented with 5% heat-inactivated fetal bovine serum and 2.5% horse serum (27). The MA-10-derived wild-type (WT) subcell lines and the *Tspo* genome-edited subcell lines nG1 and G2G were grown in this medium supplemented with 400 μg/mL of G418 (Roche Diagnostics, Indianapolis, IN), 100 U/mL of penicillin, and 100 μg/mL of streptomycin in 5% CO_2/air at 37°C, as described previously (28). The cells used for confocal microscopy and microplate reader studies were cultured on single 35-mm FluoroDish™ sterile culture dishes (World Precision Instruments, Sarasota, FL) or in 96-well plates (ViewPlate-96 black with optically clear bottom; PerkinElmer Canada Inc., Markham, ON, Canada).

CRISPR/Cas9–mediated genome editing of *Tspo* genes in MA-10 cell lines

Two guide RNAs (gRNAs) specifically targeting *Tspo* exon2 were designed using the CRISPR gRNA Design Tool (https://www.atum.bio). They were cloned into the GeneArt® CRISPR Nuclease Vector with OFP Reporter (Thermo Fisher Scientific, Mississauga, ON, Canada) through annealing of the following two oligonucleotides: *Tspo*-gRNA#1 – gRNA1-Rn: 5′-GCCTACTTTGTACGTGGCGAGTTTT-3′ and gRNA1-Fn: 5′-TCGCCACGTACAAAGTAGGCCGGTG-3′; *Tspo*-gRNA#2 – gRNA2-Rn: 5′-GCAAGCTAGCATACCACCGGGTTTT-3′ and gRNA2-Fn: 5′-CCGGTGGTATGCTAGCTTGCCGGTG-3′. The orange fluorescent protein (OFP) reporter allows for the transient expression of the OFP needed for fluorescence-based tracking of transfection efficiency and fluorescence-activated cell sorting (FACS)–based sorting/enrichment of Cas9- and CRISPR-expressing cells. All the plasmids that contained the gRNAs were confirmed by sequencing, using U6 forward sequencing primer 5′-GGACTATCATATGCTTACCG-3′. The verified plasmids were purified with a Qiagen Endofree Maxi-Prep Kit (QIAGEN, Germantown, MD).

To monitor mitochondrial activity, we established a subcell line derived from MA-10 cells, designated Mito-H, in which a mitochondrial reduction-oxidation sensitive green fluorescent protein 1 (Mito-roGFP) was stably expressed (28). The Mito-H cells expressed high levels of Mito-roGFP and formed progesterone in response to dbcAMP (28). Mito-H cells were cultured overnight in six-well plates to 80% confluence and then transfected with the GeneArt CRISPR Nuclease Vector with OFP Reporter containing each *Tspo*-specific gRNA using

Lipofectamine 2000 (Invitrogen, Carlsbad, CA) according to the manufacturer's instructions. After 24-hour transfection, the cells were subjected to FACS using BD FACSAria Fusion (five lasers, 18 parameters; BD Biosciences, San Jose, CA), and the positive cells were sorted and expanded. *Tspo* deletion was confirmed by polymerase chain reaction of genomic DNA using the *Tspo*-specific primers Exon2-R, 5′-TCAGATCTTTCCAGAACATCAGTTGC-3′ and Exon2-F, 5′-TGGCACCTACAACTACCTACCCCATGG-3′ and reverse transcription polymerase chain reaction using primers TSPO-R, 5′-GCGAAGCTTCGATGCCTGAATCCTGGGTGCC-3′ and TSPO-F, 5′-GCGGGATCCCTCACTCTGGGAGCCGGGAGCC-3′. Immunoblotting assay was performed using commercial anti-TSPO antibodies (Abs) (Table 1), and immunofluorescence was carried out using a laser-scanning confocal microscopy imaging system and epifluorescence microscopy.

Radioimmunoassay

Progesterone production was determined by radioimmunoassay using antiprogesterone antisera (MP Biomedicals, Santa Anna, CA) and [1,2,6,7-^{3}H] progesterone (specific activity 94.1 Ci/mmol; PerkinElmer), as we have done previously (28). The interassay coefficient of variation for the progesterone assay was 7.5%. All measurements were further validated using the solid-phase enzyme immunoassay. All samples were assayed in triplicate. Mean values of progesterone in medium from four biological replicates ranged between 25.19 and 326.65 pg/mL, and the %B/B_0 values were from 44.6% to 78.5%, which are within the 20% to 80% B/B_0 range. Progesterone production was normalized to the amount of protein in each well and quantified using the Bio-Rad Protein Assay reagent (Bio-Rad Laboratories Ltd., Mississauga, ON, Canada). Radioimmunoassay data were analyzed using GraphPad Prism (version 5.02; GraphPad Software, La Jolla, CA).

Neutral lipid staining and measurement

Neutral lipid staining was performed using Nile red (also known as Nile blue oxazone; AAT Bioquest, Inc., San Francisco, CA). To this end, cells were incubated at 37°C for 10 minutes in a solution of Nile red in dimethyl sulfoxide (DMSO) diluted 1:200 in serum-free OPTI medium (Invitrogen). Cells were observed by confocal microscopy to monitor fluorescence change at excitation/emission (Ex/Em) = 488/528 nm. The stained LDs were quantified using ImageJ software (https://imagej.nih.gov/ij/).

Mitochondrial staining and transmission electron microscopy imaging

To stain mitochondria, the cells were grown to 50% confluence, treated with 1 mM of dbcAMP for 2 hours, and then stained with MitoTracker Red CMXRos (Invitrogen) for 20 minutes at 37°C. Live cells were observed by Zeiss LSM780 inverted laser scanning confocal microscopy (Carl Zeiss Microscopy LLC, Thornwood, NY). Transmission electron microscopy (TEM) imaging was performed at the Facility for Electron Microscopy Research of McGill University (7). In brief, subcell lines were fixed in 2.5% glutaraldehyde in 0.1 M of sodium cacodylate buffer, postfixed in 1% OsO_4, and examined by TEM (Tecnai™ 12; FEI, Hillsboro, OR).

Table 1. Table of Information About Antibodies

Peptide/ Protein Target	Antigen Sequence (if Known)	Name of Antibody	Manufacturer: Catalog No., or Name of Source; RRID	Species Raised in; Monoclonal or Polyclonal	Dilution Used (IF, IB)
TSPO		Anti-TSPO [EPR5384]	Abcam: ab109497; RRID: AB_10862345	Rabbit	1:100 (IF) 1:1000 (IB)
STAR		Anti-STAR (FL-285)	Santa Cruz Biotechnology Inc.: sc-25806; RRID: AB_2115937	Rabbit	1:1000 (IF)
CYP11A1		Anti-CYP11A1	Abcam: ab175408; RRID: AB_2721042	Rabbit	1:1500 (IB)
Rabbit IgG		Anti-Rabbit IgG (H+L) Secondary Antibody conjugated with Alexa Fluor® 546	Thermo Fisher: A10040; RRID: AB_2534016	Donkey	1:100 (IF)
HPRT		Anti-HPRT	Abcam: ab10479; RRID: AB_297217	Rabbit	1:1300
COX IV		Anti-COX IV	Abcam: ab16056; RRID: AB_443304	Rabbit	1:1300
GAPDH		Anti-GAPDH	Trevigen: 2275-PC-100; RRID: AB_2107456	Rabbit	1:5000
Rabbit IgG		HRP-linked antibody	Cell Signaling Technology: #7074; RRID: AB_2099233	Goat	1:1300
Mouse IgG		HRP-linked antibody	Cell Signaling Technology: #7076; RRID: AB_330924	Horse	1:1300
Biotin		HRP-linked antibody	Cell Signaling Technology: #7075; RRID: AB_10696897	Goat	1:3000
Rabbit IgG		Rabbit IgG (H+L)	Molecular Probes: A10040; RRID: AB_2534016	Donkey	1:500
Mouse IgG		Anti-mouse IgG (H+L)	Molecular Probes: P31582; RRID: AB_10374586	Goat	1:500
Goat IgG		Anti-goat IgG (H+L)	Molecular Probes: A-11055; RRID: AB_142672	Donkey	1:500

Abbreviations: GAPDH, glyceraldehyde-3-phosphate dehydrogenase; HPRT, hypoxanthine-guanine phosphoribosyltransferase; IB, immunoblotting; IF, immunofluorescence; IgG, immunoglobulin G; RRID, Research Resource Identifier.

Mitochondrial $\Delta\psi_m$, redox measurement, and high-content imaging

To assay mitochondrial $\Delta\psi_m$, MA-10 and MA-10–derived cells were washed with reduced-serum medium (Opti-MEM; Thermo Fisher Scientific), treated without or with 1 mM of dbcAMP for 2 hours, and then stained with JC-10 (1:600) for 30 minutes. The plates were read using the PerkinElmer EnSpire Multimode Plate Reader with Ex/Em = 485/534 nm or 540/570 nm. The same plates were imaged using the ImageXpress micro XLS wide-field high-content analysis system (Molecular Devices, Sunnyvale, CA) or an ultra-confocal high-content analysis system to validate the plate readings. For HH and G2G subcell lines with stable Mito-roGFP expression, $\Delta\psi_m$ was measured using the TMRE–Mitochondrial Membrane Potential Assay Kit (Abcam, Toronto, ON, Canada). Tetramethylrhodamine ethyl ester (TMRE) was used to treat the cells without or with carbonyl cyanide 4-(trifluoromethoxy)phenylhydrazone (FCCP), an ionophore uncoupler of oxidative phosphorylation that eliminates membrane potential ($\Delta\psi_m$). After staining with 200 nM of TMRE for 20 minutes, measurements were performed with Ex/Em = 549/575 nm and 361/486 nm. As control, 20 μM of FCCP was added before the staining/measurement.

The same assays were performed under different treatments and time periods. The treatments included incubation with PK 11195 [1-(2-chlorophenyl)-*N*-methyl-*N*-(1-methylpropyl)-3-isoquinolinecarboxamide; Sigma-Aldrich Canada Ltd., Oakville, ON, Canada] used at 100 nM in medium from 100 mM of stock solution in DMSO; XBD173 (AC-5216; Emapunil; Tractus Chemical, Hong Kong, China) at 20 μM in medium from 5 mM of stock solution in DMSO; H-89 dihydrochloride hydrate (Sigma-Aldrich) used at 1 and 10 μM in medium from 10 mM of stock solution in DMSO; or paclitaxel (Sigma-Aldrich Canada Ltd.) at 100 nM in culture medium from 1 mM of stock solution in DMSO. Cells were treated with PK 11195, XBD173, or paclitaxel for 4 hours or with H-89 for 30 minutes before the $\Delta\psi_m$ measurements were undertaken.

Laser scanning confocal microscopy

For live cell staining of microtubules, the cells were stained with MitoTracker Red CMXRos (Invitrogen; Ex/Em: 579/599) for 20 minutes and then with TubulinTracker™ Green (Oregon Green® 488 Taxol, bis-acetate; Ex/Em: 494/522 nm) (Thermo Fisher Scientific) for 30 minutes (37°C), as described by the manufacturer. For live cell staining of STAR protein, the cells were transfected with the plasmids encoding a mitochondria-targeted blue fluorescent protein (Ex/Em: 402/457 nm) and STAR-DsRed monomer (Ex/Em: 557/592 nm) overnight and then incubated with MitoTracker® Deep Red FM (Invitrogen; Ex/Em: 644/665 nm) for 20 to 30 minutes. The stained cells were viewed by confocal microscopy.

For immunofluorescence staining, the cells were fixed in a 4% paraformaldehyde solution plus 0.1% Triton X-100 in phosphate-buffered saline (PBS) for 5 minutes and washed in PBS for 5 minutes. After blocking with 1% bovine serum albumin in PBS plus 10% donkey normal serum for 30 minutes at 37°C, the cells were incubated with rabbit anti-TSPO monoclonal Ab [EPR5384] (Abcam) overnight and then with Donkey anti-Rabbit IgG (H+L) Secondary Antibody conjugated with Alexa Fluor® 546 (Thermo Fisher Scientific) for 1 hour at room temperature (Table 1). Cells were mounted using UltraCruz® Aqueous Mounting Medium containing 4′,6-diamidino-2-phenylindole (Santa Cruz Biotechnology, Dallas, TX). Cells were imaged with the Olympus Fluoview™ FV1000 laser confocal microscope and Olympus IX51 inverted epifluorescence microscope (Tokyo, Japan) and/or a Zeiss LSM780 inverted laser scanning confocal microscope (Carl Zeiss Inc.). Images were analyzed by ImageJ software (https://imagej.nih.gov/ij/).

Detection of caspase-3/7 activity and cell proliferation and viability assay

To assess whether the reduced progesterone production in cells with TSPO deficiency was due to programmed cell death induced by the dbcAMP treatment, we treated the cells with dbcAMP for 2 hours, then added CellEvent™ caspase-3/7 green detection reagent (1:600; Thermo Fisher Scientific) for 30 minutes before imaging with the Olympus Fluoview™ FV1000 laser confocal microscope. Apoptotic cells (green) and nonapoptotic cells (counterstained blue) were counted using Image-Pro 6.3 (Media Cybernetics Inc., Silver Spring, MD). Cell proliferation assays were performed using the WST-1 colorimetric test, which measures mitochondrial dehydrogenase activity by the cleavage of the tetrazolium salt WST-1 to form a red formazan dye by viable cells (Cell Proliferation Reagent WST-1; Roche). Cells were seeded at the same density in serum-free media. Cell density per well before and after dbcAMP treatment was assessed by collecting OD450nm/620 nm values using the Victor™ X5 2030 Multilabel Reader (PerkinElmer, Waltham, MA).

Immunoblot analysis

Total protein extracts for immunoblot analysis were prepared from MA-10 cells and its derived cell lines using M-PER Mammalian Protein Extraction Reagent (Thermo Fisher Scientific). After centrifugation, protein concentration was quantified using the Bradford dye assay (Bio-Rad Laboratories Ltd.). Sodium dodecyl sulfate-polyacrylamide gel electrophoresis and immunoblot analysis were performed as previously described (29). In brief, 20 μg of protein extract was subjected to sodium dodecyl sulfate-polyacrylamide gel electrophoresis using a 4% to 20% Tris-glycine gradient gel (Invitrogen) and electrotransferred to a polyvinylidene fluoride membrane. Membranes were blocked in 10% fat-free milk overnight and incubated with primary Abs specific for TSPO, glyceraldehyde-3-phosphate dehydrogenase, hypoxanthine-guanine phosphoribosyltransferase, STAR, CYP11A1, or COX IV, followed by anti-rabbit immunoglobulin-G horseradish peroxidase-conjugated secondary Ab (Cell Signaling Technology, Danvers, MA). Information about the Abs and dilutions used are provided in Table 1. In the case of anti-STAR immunoblot, the membranes were stripped of the Ab using Restore™ Western Blot Stripping Buffer (Thermo Fisher Scientific) and were reprobed using anti-COX IV. Immunoreactive proteins were visualized using the Amersham ECL Western Blotting Detection Reagent (GE Healthcare Life Sciences, Mississauga, ON, Canada), and images were captured using a FUJI image reader LAS4000 (Fujifilm, Tokyo, Japan).

Molecular modeling

The predicted secondary structure of TSPO was produced using TMRPres2D (30). The molecular surfaces of WT TSPO

(PDB: 2MGY) were produced after removal of PK 11195 and with minimized energy in the Swiss-PdbViewer (V.4.1) (31, 32).

Statistical analysis

Data were expressed as mean ± standard error of the mean, and graphic presentation was performed using GraphPad Prism (version 5.02; GraphPad Software) for Windows. Statistical analyses of data were performed by the unpaired Student *t* test. Mean differences were considered statistically different when $P < 0.05$.

Results

CRISPR/Cas9–mediated *Tspo* deletion mutation in MA-10 cells

To generate *Tspo* mutant/deleted cell lines, we designed two gRNAs specifically targeting *Tspo* exon2. The two, gRNA1 (in red) and gRNA2 (in green), were cloned into the GeneArt® CRISPR Nuclease Vector with OFP Reporter (Fig. 1A and 1B). After their transfection into cells of the MA-10 subline Mito-H, we performed FACS analysis that resulted in four major groups of cell populations [quarter (Q) 1, Q2, Q3, and Q4]: G1, cells expressing OFP without detectable gene deletion; nG1, cells expressing OFP with detectable *Tspo*-targeted gene deletion; G2G, cells expressing both Mito-roGFP and OFP with *Tspo*-targeted gene deletion; and HH, cells expressing Mito-GFP without *Tspo* gene deletion (Fig. 1C and 1D). The *Tspo*-specific gene deletions were confirmed by locus-specific polymerase chain reaction and sequencing in comparison with the WT gene sequence (Supplemental Fig. 1A–1C). The characteristics of each MA-10–derived subcell line are summarized in Table 2. After expansion of the cell colonies, immunoblotting analyses were performed to validate the TSPO protein depletion or mutation. The results showed that no immunoreactive TSPO protein could be detected in G2G cells (Supplemental Fig. 1D), a result supported by reverse transcription polymerase chain reaction analysis showing that the sizes of corresponding messenger RNA shifted, especially in the nG1 cells (Supplemental Fig. 1E). In addition, immunoblotting analysis of the nG1 cells showed that the 18 kDa TSPO protein monomer disappeared, although a higher molecular weight immunoreactive TSPO polymer appeared (Supplemental Fig. 1F). We also assessed whether the expression levels of CYP11A1, the mitochondrial enzyme that catalyzes conversion of cholesterol to pregnenolone, were affected by the genome editing system. The results show that the subcell line contained CYP11A1 at levels equal to those of WT cells (Supplemental Fig. 1G). These data suggest that *Tspo* in both nG1 and G2G was successfully mutated using the CRISPR/Cas9 methodology, resulting in depletion of the 18 kDa TSPO or dramatic reduction of its expression.

Immunofluorescence analyses of WT and *Tspo*-deleted cell lines by confocal laser scanning microscopy and epifluorescence microscopy show that the WT TSPO was expressed on the OMM (Fig. 1E, 1G, 1I, and 1K; Supplemental Fig. 2A and 2C). However, in the *Tspo* mutant cells, there were no or very few cells stained by the anti-TSPO Ab (Fig. 1F, 1H, 1J, and 1L; and Supplemental Fig. 2B and 2D). These data suggest that TSPO was mutated and/or depleted in the MA-10 subcell lines nG1 and G2G, whereas the expression of TSPO in the corresponding original MA-10 subcell lines G1 and HH was not affected.

TSPO deficiency inhibited dbcAMP-stimulated progesterone production

The sequence alignment of the targeting regions from WT, nG1, and G2G cells indicated the deletion of four nucleotide acids, "GTGG," in G2G and 26 nucleotide acids, "TGTACGTGGCGAGGGCCTCCGGTGGT," in nG1 (Fig. 2A). The corresponding open reading frames were aligned to show that both *Tspo* mutant cells likely encode an *N*-terminal truncated protein, as shown in the amino acid sequence alignment (Fig. 2B) and secondary structure of the WT TSPO (Supplemental Fig. 3A). Nevertheless, the mutant TSPO from both cell lines, if any was expressed, may not have functioned the same as WT TSPO because its molecular surface would be changed from a positive potential to a neutral potential (Supplemental Fig. 3B).

To examine the effect of mutant TSPO on Leydig cell steroid biosynthesis, we assessed progesterone production by nG1 and G2G cells under basal conditions and in response to dbcAMP treatment. There were no significant changes in basal progesterone production between TSPO mutant nG1 and G2G cells compared with their respective control G1 and HH cells (Fig. 2C and 2E). However, progesterone production in response to dbcAMP treatment was abolished in nG1 cells compared with control G1 cells (Fig. 2D) and was significantly reduced, by 60% in G2G cells compared with their control HH cells (Fig. 2F).

TSPO deficiency led to neutral lipid accumulation after dbcAMP stimulation

To interpret reduced progesterone biosynthesis by cells with TSPO deficiency, we speculated that the free cholesterol used for steroid biosynthesis would accumulate in the cytosol. In steroidogenic cells, free cholesterol can be stored in LDs containing a neutral lipid core surrounded by a phospholipid monolayer and associated proteins (33). We used Nile red to stain the neutral lipids in LDs (Fig. 2G–2J). In control G1 cells, dbcAMP stimulation resulted in significant reduction in

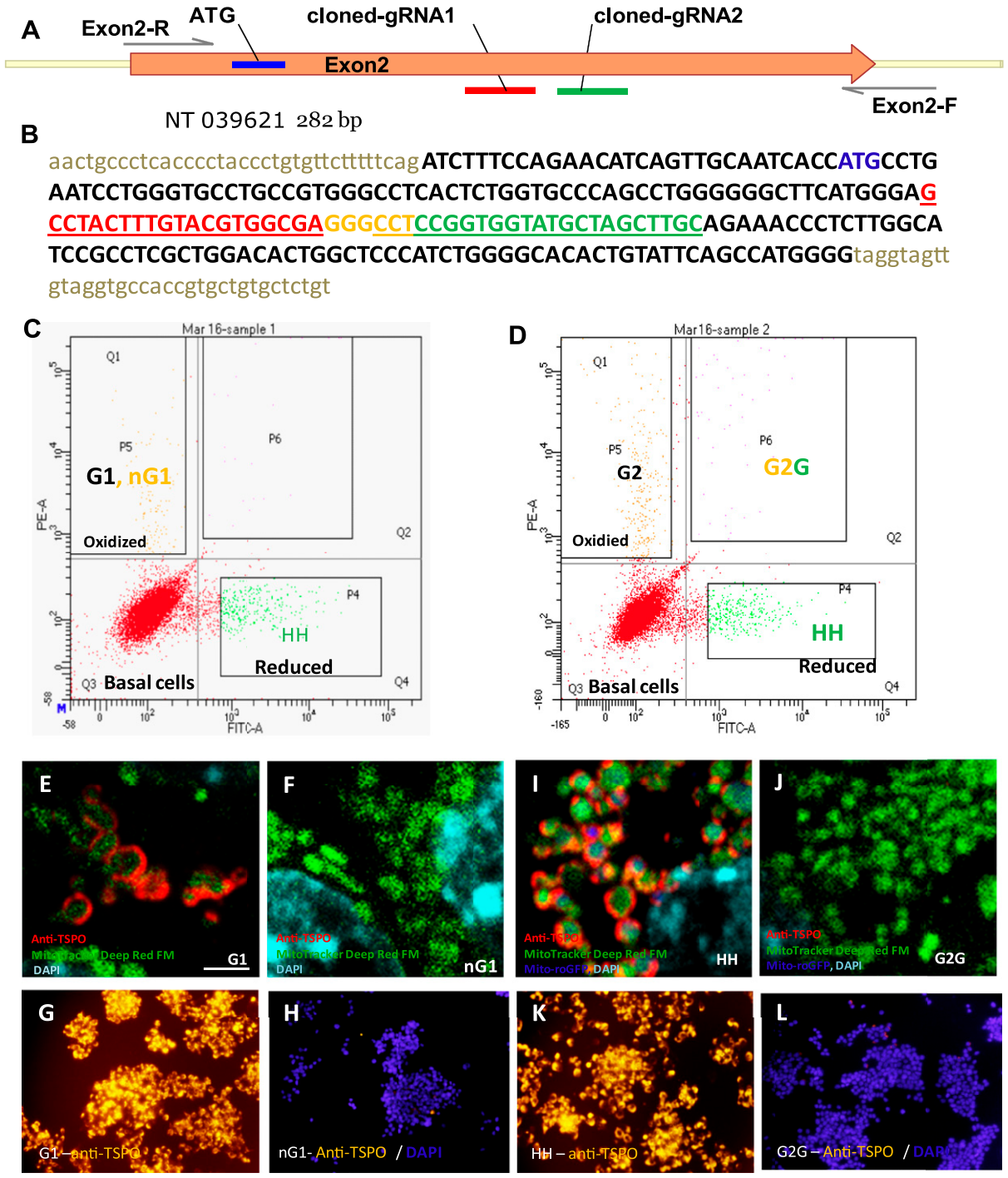

Figure 1. Screening and validation of CRISPR/Cas9–mediated *Tspo* mutant MA-10 mouse Leydig cells. (A) Two gRNAs, cloned-gRNA1 and cloned-gRNA2, were designed within exon2 of the *Tspo* gene after the codon ATG. Exon2-R and Exon2-F were the primers used for screening of mutant genomic DNAs. (B) Exon2 and its flanking sequences are shown. Red, gRNA1; green, gRNA2; orange, the gap between gRNA1 and gRNA2. Bold letters, exon2; small letters, intron sequence. (C, D) Cell sorting of the Mito-H cells [MA-10 cells expressing Mito-roGFP (28)] transfected with the two plasmid constructs from (C) gRNA1 and (D) gRNA2 for 24 hours was performed by FACS. The resulting graphs show the four subpopulations of cells in scattergrams: G1/nG1 (Q1), the transfected cells lacking Mito-roGFP; G2G (Q2), the transfected cells expressing Mito-roGFP; basal (Q3) cells expressing Mito-roGFP; and HH (Q4), cells with higher expression of Mito-roGFP. (E–L) Immunofluorescence (IF) staining of TSPO in the CRISPR/Cas9–mediated mutant cells nG1 and G2G in comparison with the WT cells G1 and HH, respectively. The IF was performed using laser scanning confocal microscopy as well as epifluorescence microscopy in WT cells [(E) and (G) for G1; (I) and (K) for HH] and in mutant cells [(F) and (H) for nG1; (J) and (L) for G2G]. TSPO was labeled with rabbit monoclonal anti-TSPO Ab and Alexa Fluor® 546 Donkey Anti-Rabbit IgG (E, F, I, and J) in red for confocal images and (G, H, K, and L) in yellow for epifluorescence images. Original images for highlighted areas in panels E, F, I, and J are presented in Supplemental Fig. 2. (H, L) The merged channel of red/blue, where only a few G2G cells have very weak staining for TSPO or background staining, is shown; the nucleus was counterstained in blue using DAPI. Mitochondria were counterstained with MitoTracker™ Deep Red FM and painted in green and are also shown by Mito-roGFP in blue for cells HH and G2G. Scale bars: 5 μm for confocal images and 100 μm for epifluorescence images. DAPI, 4′,6-diamidino-2-phenylindole; IgG, immunoglobulin-G.

Table 2. MA-10 Cells (WT) and Derived Cell Lines Used in This Study

MA-10 Cell/Characteristics	Mito-roGFP[a]	OFP[b]	*Tspo*
WT	−	−	+
Mito-H	+	−	+
G1	−	+/−	+
nG1	−	+/−	−
G2G	++	+/−	−
HH	++	−	+
Basal	−	−	+

Abbreviations: −, no expression; +, expression; ++, strong expression; +/−, transient expression.

[a]Mito-H, a stable cell line expressing Mito-roGFP; Mito-HH, a stable cell line expressing Mito-roGFP after resorting the Mito-H cells using an excitation wavelength of 488 nm.

[b]The expression of OFP is transient; OFP will be absent after the expansion of the cell line(s).

LDs, suggesting that LDs were used to supply cholesterol for steroidogenesis. In contrast, there was a significant increase in LD numbers in dbcAMP-stimulated TSPO-deficient nG1 cells (Fig. 2K). These data suggest that the free cholesterol used for steroid biosynthesis was compromised in the TSPO-deficient cells, leading to LD accumulation.

TSPO deficiency resulted in changes in mitochondrial morphology and in OMM and IMM contact sites and/or fusion

MitoTracker probes are cell-permeable, mitochondria-selective dyes that passively diffuse across the plasma membrane and accumulate in active mitochondria. We used these probes to examine whether there are changes in mitochondrial morphology in cells depleted of TSPO. Untreated cells or cells treated with dbcAMP were stained with Mitotracker Red CMXRos (Invitrogen) (Fig. 3; Supplemental Fig. 4). Mitochondrial morphology in G1 (Fig. 3A–3C) and nG1 (Fig. 3D–3F) cells in response to dbcAMP treatment differed with mitochondrial swelling seen in nG1 cells (compare Fig. 3C with Fig. 3F).

We then examined subcellular features of the mitochondria by TEM. In the control G1 cells, the mitochondrial membranes were distinct and of high density. The membranes became more diffuse after the cells were treated with dbcAMP (Fig. 3G and 3H). These observations are consistent with those from MitoTracker staining (Fig. 3C). In TSPO-depleted nG1 cells, the two mitochondrial membranes were separate but with a number of contact sites (Fig. 3I). After dbcAMP treatment, the OMM and IMM of these cells were fused (Fig. 3J). In contrast to analysis of nG1 cells, confocal and TEM analyses of TSPO-depleted G2G cells indicated that there were no remarkable changes in mitochondrial morphology from the control HH cells. However, staining with MitoTracker differed somewhat between G2G and HH cells, appearing more in the periphery rather than inside the mitochondria in G2G cells (Supplemental Fig. 4).

The Mito-roGFP1 probe in Mito-H cells and its subcell lines is in dynamic equilibrium with the mitochondrial redox status and responds to membrane-permeable reductants and oxidants (35). Thus, Mito-roGFP (in green), which was used to monitor the redox status, was counterstained with MitoTracker (Supplemental Fig. 4B, 4D, 4G, and 4H). Although control HH cells treated with dbcAMP showed reduced roGFP staining at 480 nM, indicating changes in the mitochondrial redox conditions (Supplemental Fig. 4B and 4D), there was no change in TSPO-depleted G2G cells (Supplemental Fig. 4F and 4H). These observations are consistent with the direct measurement of redox status (400/488 ratio) between these two cell lines and indicate that the presence of TSPO is related to mitochondrial redox homeostasis (see later).

TSPO deficiency resulted in reduced mitochondrial $\Delta\psi_m$

The cationic and lipophilic JC-10 dye, a derivative of JC-1 (5,5′,6,6′-tetrachloro-1,1′,3,3′-tetraethylbenzimidazoyl carbocyanine iodide), has been widely used to monitor mitochondrial health *via* its reversible changes from red fluorescence in normal cells to green fluorescence in apoptotic and necrotic cells as membrane potential decreases (36–38). JC-10 staining was performed to assess changes in mitochondrial $\Delta\psi_m$ in the control and TSPO-mutant cells. $\Delta\psi_m$ was significantly reduced in the TSPO-deficient nG1 cells compared with the control G1 cells. Treatment with dbcAMP further reduced $\Delta\psi_m$ in nG1 cells (Fig. 4A). Examination of the stained cells from high-content imaging similarly revealed mitochondrial color shift from red to green with TSPO depletion (compare Fig. 4B with Fig. 4C) and after dbcAMP treatment (compare Fig. 4D with Fig. 4E). In HH and G2G cells expressing Mito-roGFP, we used TRME staining, which emits red fluorescence, to assess changes in $\Delta\psi_m$. The results showed that $\Delta\psi_m$ was significantly reduced in TSPO-deficient G2G compared with control HH cells (Fig. 4F). However, the reduced $\Delta\psi_m$ was not as low as that seen using the mitochondrial oxidative phosphorylation uncoupler (FCCP) or as much as that seen in nG1 cells, where TSPO expression was absent (Fig. 4E and 4A). These results indicate that TSPO deficiency leads to mitochondrial depolarization.

Decreased $\Delta\psi_m$ and progesterone synthesis in *Tspo* mutant cells were TSPO specific

Two TSPO-specific ligands, PK 11195 (100 nM; Sigma-Aldrich Canada Ltd.) and XBD173 (20 μM; Tractus Chemical), were used to treat cells. Both compounds

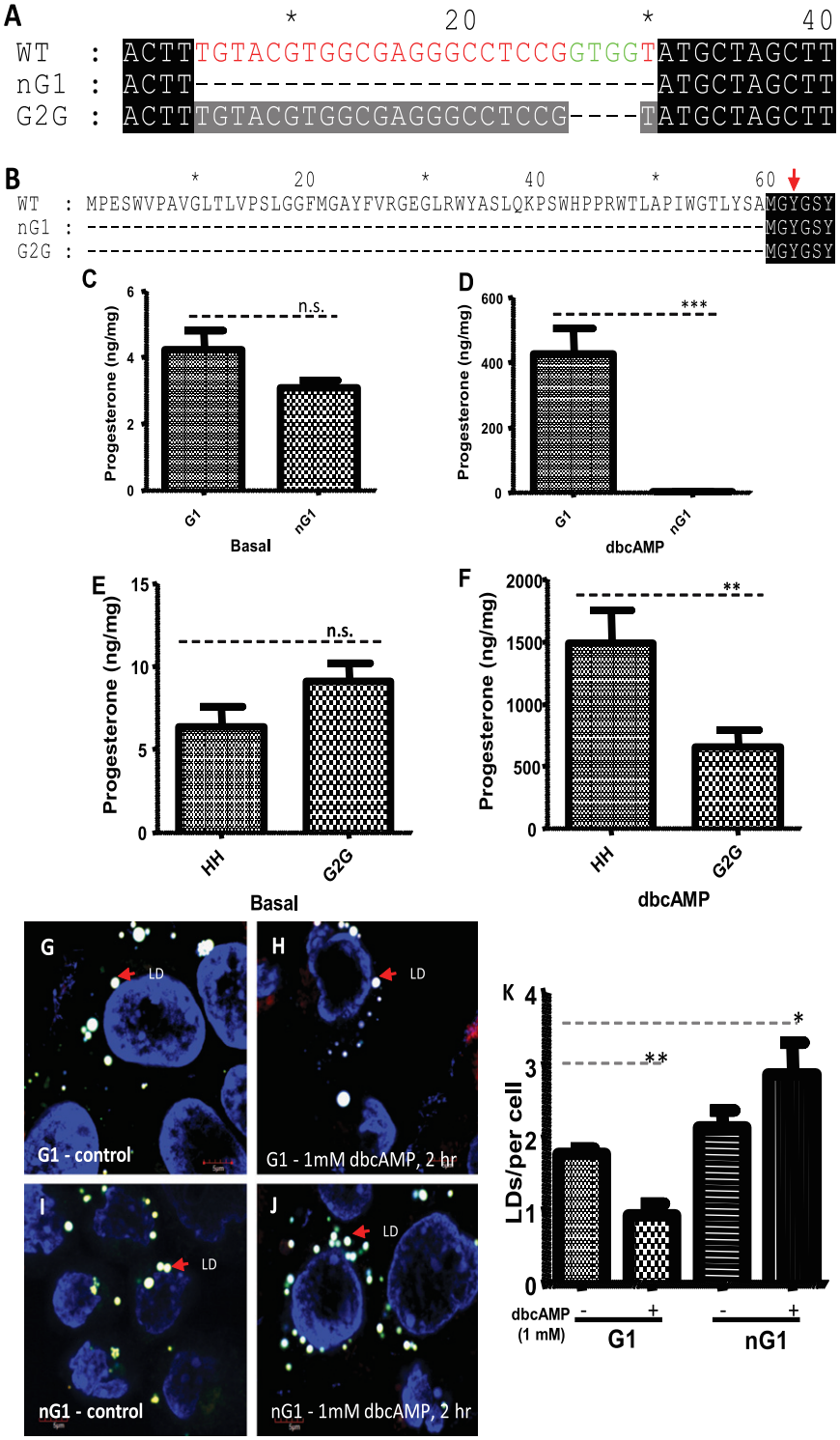

Figure 2. Genomic structure, predicted truncated peptides, defective steroid biosynthesis, and altered neutral lipid homeostasis in the *Tspo* mutant cells nG1 and G2G. (A) Genomic sequence alignments of nG1, G2G, and WT *Tspo* loci around the CRISPR/Cas9 targeting area. Dashes indicate the deletion of 26 nucleotides in nG1 cells and four nucleotides in G2G cells. (B) Predicted peptides of mutant TSPO in nG1, G2G, and WT cells. The second likely methionine (M60) seems to be present in both mutant nG1 and G2G cells. Dashes indicate the gaps introduced for sequence alignment or the missing amino acids in the predicted mutant proteins. Red arrow indicates one of the two tyrosines forming the covalent bound in TSPO dual topology model. (C, D) Disrupted stimulated progesterone production in nG1 vs G1 cells: (C) control vs (D) dbcAMP treatment. (E, F) Reduced stimulated progesterone production in G2G vs HH cells: (E) control vs (F) dbcAMP treatment. Results shown are means ± standard error of the mean (SEM; n = 4). (G–K) TSPO deficiency led to increased cytosolic neutral lipid accumulation in the cells after dbcAMP treatment. (G, H) The LDs include esterified cholesterol stained with Nile Red in G1 cells (G) before and (H) after dbcAMP treatment. (I, J) LDs include esterified cholesterol stained with Nile red in nG1 cells (I) before and (J) after dbcAMP treatment. Red arrows indicate representative LDs in white. (K) Quantification of LDs per cell among the cells used: G1 control, G1 with dbcAMP treatment, nG1 control, and nG1 with dbcAMP treatment. Results shown are means ± SEM (n = 386). $*P < 0.05$; $**P < 0.01$; $***P < 0.001$ by Student *t* test. n.s., no significance.

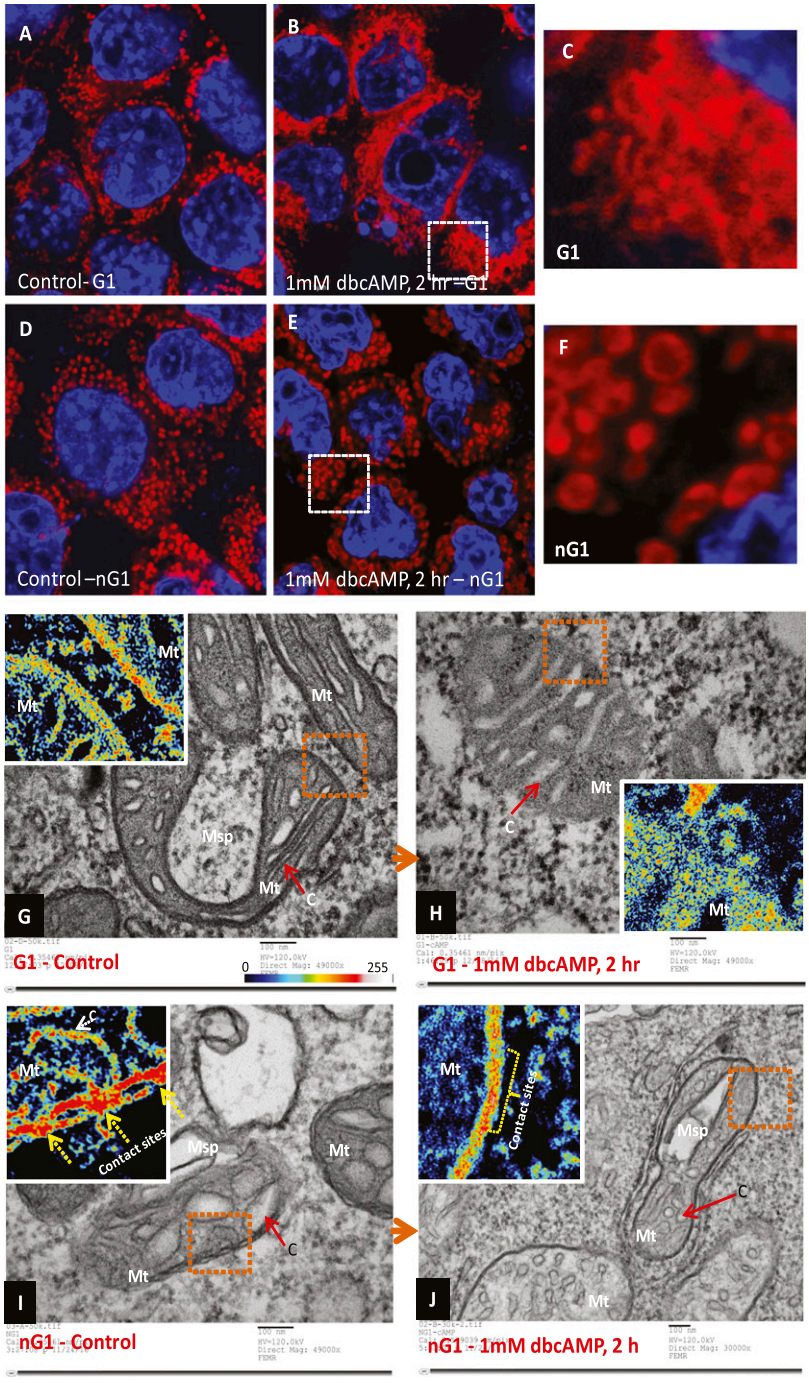

Figure 3. TSPO depletion affected mitochondrial membrane structure and morphology. (A–F) The live mitochondria in G1 and nG1 cells were stained with Mitotracker Red CMXRos (Invitrogen), which depends on $\Delta\psi_m$ (A, D) before and (B, E) after dbcAMP treatment. (C, F) The magnified areas after dbcAMP treatment, where the staining of mitochondria in G1 cells was diffused, are highlighted, which may be correlated with the mitochondrial fusion that has been related with steroidogenesis (34); the staining of mitochondria in nG1 cells is shown in "ballooning" or swelling shapes, indicating that there was a dramatic change in mitochondrial morphology or $\Delta\psi_m$ after TSPO depletion. (G–J) TEM of fixed mitochondria from the same cells as indicated in (A–F). Indel, imaging the intensity of the highlighted area painted in pseudocolor according to the reference bar. (G, H) The mitochondrial double membrane barrier is clearly seen in the G1 cells, but the boundary is blurred after dbcAMP treatment. (I, J) However, in the nG1 cells, the contact sites between the OMM and IMM are clearly seen (yellow arrows and lines); the membranes are clearly seen as a boundary between the mitochondria and cytoplasm after cAMP stimulation. The mitochondrial spheroids (Msp) or mitophagy (Mtp) are also indicated. The red arrows indicate the mitochondria (Mt); the Cristae membrane is indicated.

significantly enhanced $\Delta\psi_m$ in control cells but not in cells with mutated *Tspo* (Fig. 5A and 5B). The cyclic adenosine monophosphate (cAMP)–dependent protein kinase (PKA) inhibitor H-89 (Sigma-Aldrich), used at 1 and 10 μM, increased the $\Delta\psi_m$ in all cells examined (Fig. 5C), suggesting that the repressed $\Delta\psi_m$ in TSPO-deficient cells can be recovered. TSPO deficiency led to a significantly elevated mitochondrial oxidized condition, but no changes were seen after PK 11197 or XBD173 treatment (Fig. 5D and 5E). Treatment with dbcAMP decreased the $\Delta\psi_m$ in controls but not in TSPO-deficient cells (Fig. 5F). Under the same conditions, control HH but not TSPO-deficient G2G cells responded to PK 11195 by producing increased levels of progesterone (Fig. 5G). Moreover, although TSPO-deficient cells were characterized by low $\Delta\psi_m$, they were resistant to apoptosis and had similar relative proliferation rates before and after dbcAMP treatment (Supplemental Fig. 5).

TSPO-deficient cells lost response to the tubulin stabilizing agent paclitaxel and show reduced colocalization of mitochondria with microtubules

To investigate the mechanism of TSPO-mediated $\Delta\psi_m$ reduction, we examined the effect of the tubulin-stabilizing agent paclitaxel (Sigma-Aldrich Canada Ltd.) on TSPO-deficient cells nG1 and G2G compared with the effect on their respective control cells G1 and HH. Free tubulin has been shown to regulate $\Delta\psi_m$ in cancer cells by blocking VDAC function in a PKA-dependent manner (39–41). Free tubulin and organized microtubules were also associated with adrenocorticotropic hormone– and cAMP–stimulated steroidogenesis in murine adrenal and rat Leydig cells (42). In the current studies, paclitaxel (100 nM; Sigma-Aldrich Canada Ltd.) significantly increased the $\Delta\psi_m$ in controls by enhancing tubulin polymerization but not in TSPO-deficient cells, indicating that the TSPO-mediated $\Delta\psi_m$ regulation involved

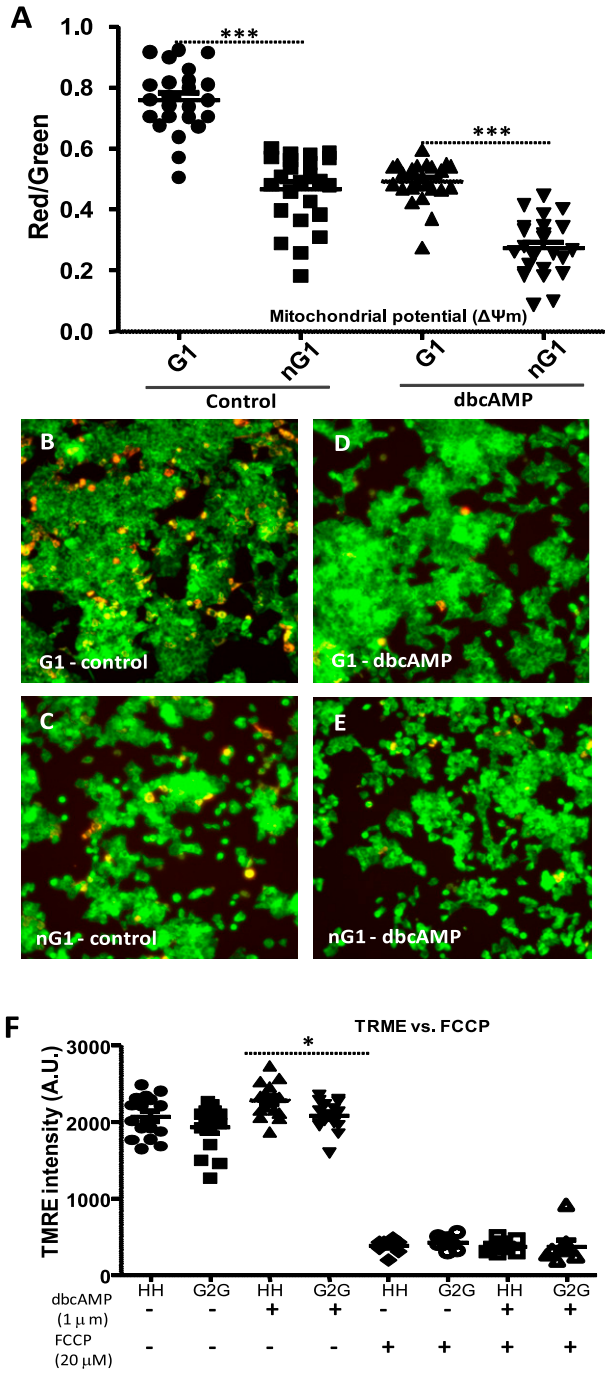

Figure 4. TSPO deficiency decreased $\Delta\psi_m$. (A) The ratio of JC-10 red/green fluorescence intensity of G1 and nG1 before and after 1-mM dbcAMP treatment was obtained from PerkinElmer EnSpire multimode plate reader. (B–E) High-content images of corresponding cells: G1 (control vs dbcAMP) and nG1 (control vs dbcAMP) from Molecular Devices ImageXpress Micro XLS wide-field high-content analysis system. Red (540/570 nm), healthy mitochondria; green (485/534 nm), depolarized or apoptotic cells. (F) Evaluation of $\Delta\psi_m$ in TSPO-deficient cells: G2G vs WT cell: HH. TMRE fluorescence intensity was graphed before and after FCCP treatment (to eliminate the $\Delta\psi_m$), where the G2G cells have a lower $\Delta\psi_m$ than the WT cells, which is the same as in the nG1 cells. Results shown are means ± standard error of the mean (n = 24). $^*P < 0.05$; $^{***}P < 0.001$ by Student *t* test.

VDAC-tubulin interaction (Fig. 6A and 6B). Data from previous mass spectrometry studies on the mitochondrial protein complex involved in steroidogenesis indicated that cytoskeletal proteins were involved in the dbcAMP treatment and that microtubule elements were lost in the lower-molecular-weight complexes, whereas the ACTG1 and vimentin proteins were upregulated in the higher molecular protein complexes (Fig. 6C) (11). A search through the protein-protein interaction network STRING (https://string-db.org/) showed that TSPO is associated with cytoskeletal proteins *via* VDAC (Fig. 6D). Confocal images of microtubules and mitochondria show that the overlap of mitochondria and polymerized tubulin was reduced in TSPO-deficient cells (Fig. 6E–6J). Fluorescence intensity analysis shown by scatter plots and a bar graph of Mander's overlap coefficient *R* also showed reduced colocalization in TSPO-deficient nG1 cells (Fig. 6K). These confocal data suggest a TSPO-mediated microtubule-mitochondria interaction most likely occurring *via* the regulation of dimeric tubulin-VDAC interaction (41, 43).

TSPO was involved in STAR protein mitochondrial import/function, which was correlated with reduced $\Delta\psi_m$ in TSPO-deficient cells

Immunoblot analysis showed the induction of STAR immunoreactive proteins in control G1 and HH cells after treatment with dbcAMP for 2 hours (Fig. 7A–7D), but to a lesser extent than that seen in the TSPO-deficient nG1 and G2G cells (Fig. 7B and 7D). The presence of increased levels of the 37-kDa cytosolic STAR and cleaved STAR protein before dbcAMP stimulation in nG1 cells suggests that although most STAR is not processed, some is imported and processed in the mitochondria (Fig. 7B). The lack of change in the pattern of STAR before and after dbcAMP treatment in G2G cells indicates that STAR accumulated outside the mitochondria (Fig. 7D); no processing occurred. These observations are most likely due to the fact that STAR can be processed only by the mitochondrial *Lon* protease after mitochondrial import (44). These data also suggest that STAR is imported into mitochondria in a TSPO-dependent fashion. Confocal imaging of STAR-DsRed protein was used to track the STAR mitochondrial import. STAR-DsRed was found to be imported into mitochondria in control G1 cells in response to dbcAMP treatment, whereas nG1 TSPO-deficient cells showed a notable amount of protein outside the mitochondria (Fig. 7E–7L). Similar results were obtained using HH control and G2G TSPO-deficient cells (Supplemental Fig. 6). Both the immunoblot analysis and confocal imaging suggest that the mitochondrial import of STAR depends on the presence of TSPO and polarized mitochondria (*i.e.*, maintenance of its $\Delta\psi_m$).

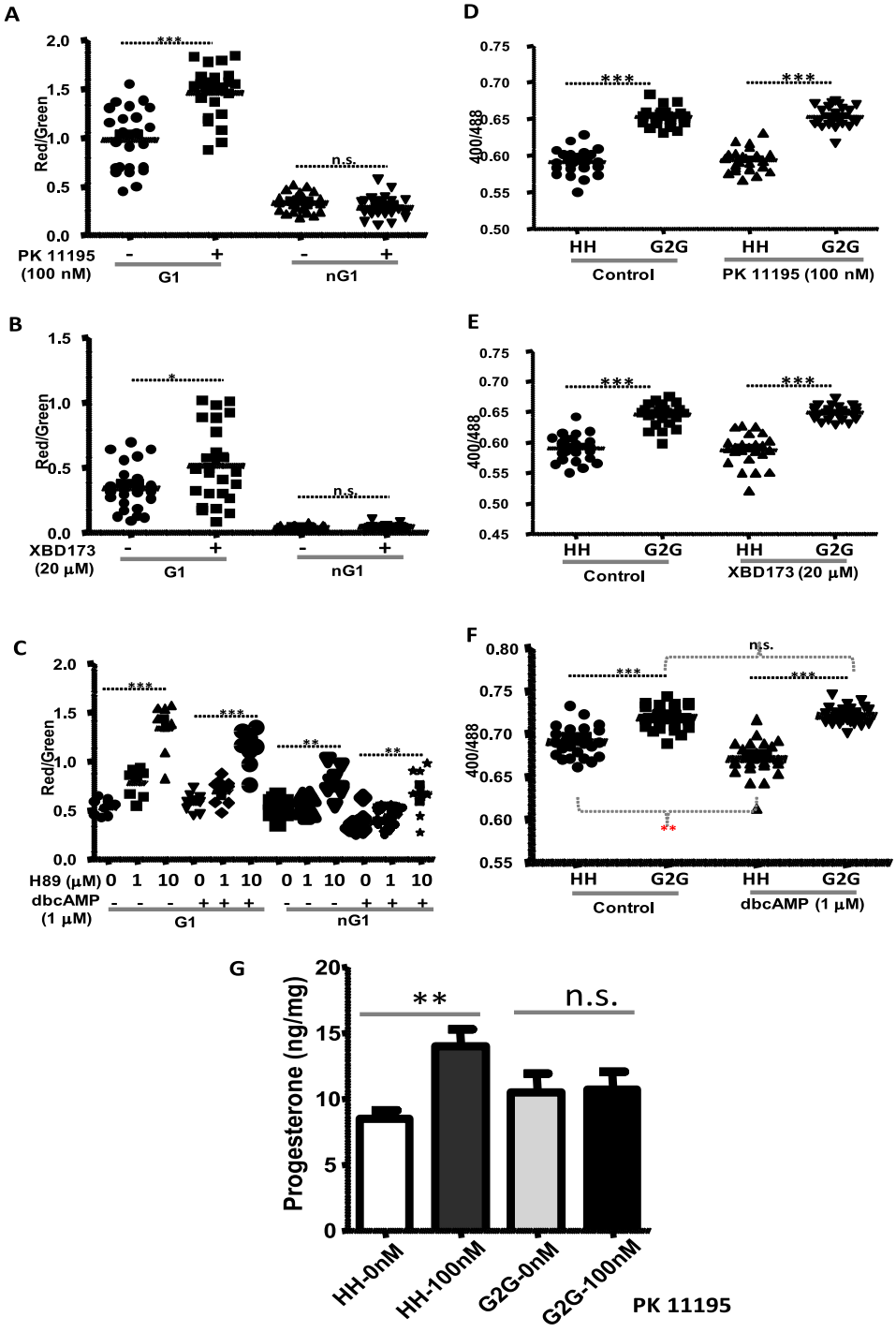

Figure 5. The reduced $\Delta\psi_m$ in TSPO-deficient cells was TSPO specific. The TSPO ligands PK 11195 (Sigma-Aldrich Canada Ltd.) and XBD173 (Tractus Chemical) increased $\Delta\psi_m$ *via* TSPO. (A) Increased $\Delta\psi_m$ after PK 11195 treatment in control G1 cells. 100 nM of PK 11195 affected the $\Delta\psi_m$ only in G1 cells, not in TSPO-deficient nG1 cells. (B) Increased $\Delta\psi_m$ after 20-μM XBD173 treatment in G1 control cells; 20-μM XBD173 affected the $\Delta\psi_m$ only in G1 cells, not in TSPO-deficient nG1 cells. (C) Recovery of the collapse of $\Delta\psi_m$ in TSPO-deficient cells by the PKA inhibitor H-89 (10 μM; Sigma-Aldrich) and effects of H-89 (1 and 10 μM) on the $\Delta\psi_m$ of G1 and nG1 cells. H-89 (10 μM) significantly increased the $\Delta\psi_m$. (D, E) No effect on mitochondrial redox status monitored by Mito-roGFP after PK 11195 (100 nM) and XBD173 (20 μM) treatments. However, the TSPO-deficient cells maintained a higher oxidized mitochondrial condition. (F) No effect of mitochondrial redox status after dbcAMP treatment of TSPO-deficient cells, but control cells kept a significantly reduced condition. Results shown are means ± standard error of the mean (SEM; n = 24). (G) PK 11195–stimulated steroid production. Control HH cells and TSPO mutant G2G cells were treated with and without PK 11196 (100 nM) for 2 hours. Progesterone formed was measured by radioimmunoassay. Results shown are means ± SEM (n = 4). $^*P < 0.05$; $^{**}P < 0.01$; $^{***}P < 0.001$ by Student *t* test. n.s., no significance.

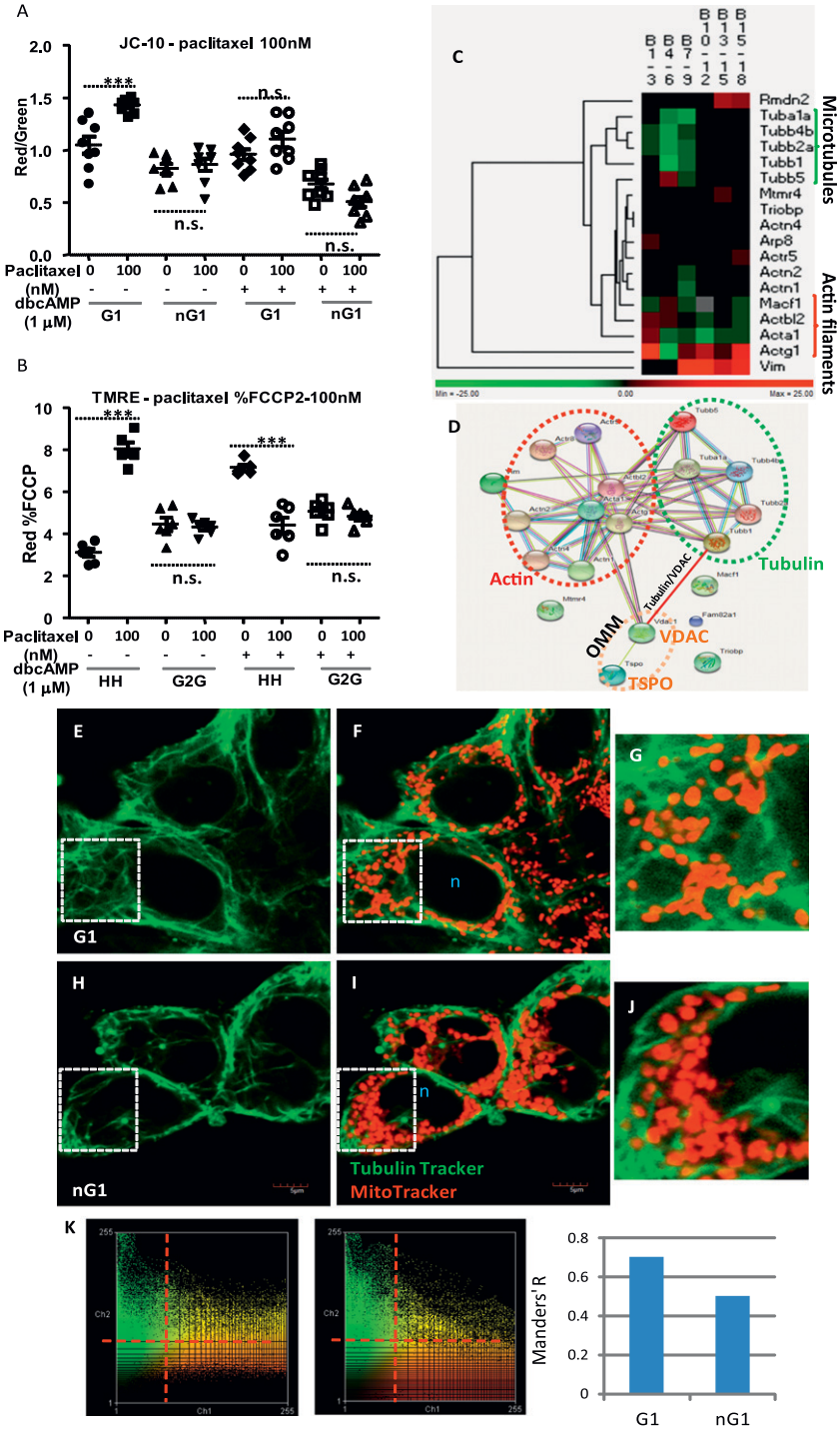

Figure 6. TSPO-mediated $\Delta\psi_m$ reduction *via* VDAC-tubulin interaction. The tubulin stabilizing agent paclitaxel (Sigma-Aldrich Canada Ltd.) increased $\Delta\psi_m$ *via* TSPO. (A) Increased $\Delta\psi_m$ after 100-nM paclitaxel treatment of control G1 cells, but lack of response in TSPO-deficient nG1 cells. (B) Significant changes in $\Delta\psi_m$ after 100-nM paclitaxel treatment of control HH cells, but no response in TSPO-deficient G2G cells. (C) Cytoskeleton proteins, including tubulins, were involved in dbcAMP-induced steroidogenesis in MA-10 cells. Microtubule-associated proteins were identified in the mitochondrial protein complexes found in bands 1 to 9, whereas actin filament–associated proteins were increased in the mitochondrial protein complexes. The mass spectrometry data were extracted from a previous study on TSPO-mediated cholesterol mitochondrial transport complexes (11). (D) The TSPO-associated cytoskeleton protein-protein interaction. The main interactions were retrieved from the STRING database (http://string-db.org), except that the VDAC-tubulin interaction is from a previous publication on dimeric tubulin blocking VDAC closure at negative potentials (40). (E–J) Confocal imaging of the overlap of polymerized tubules and mitochondria in (E–G) control G1 cells and (H–J) TSPO-deficient nG1 cells. Insets in panels (E) and (F) identify the areas shown in panel (G), and insets in panels (H) and (I) identify the areas shown in panel (J). Cells were stained with MitoTracker Red CMXRos (Invitrogen; Ex/Em: 579/599) for 20 minutes, then with the Thermo Fisher Scientific TubulinTracker™ Green (Oregon Green® 488 Taxol, bis-acetate; Ex/Em: 494/522 nm) for 30 minutes. (K) Scatter plots of two channels in G1 (left) and nG1 (right) cells and a bar graph show the Mander's overlap coefficient (*R*) value as a measure of colocalization between polymerized tubules and mitochondria. $***P < 0.001$ by Student *t* test. n.s., no significance.

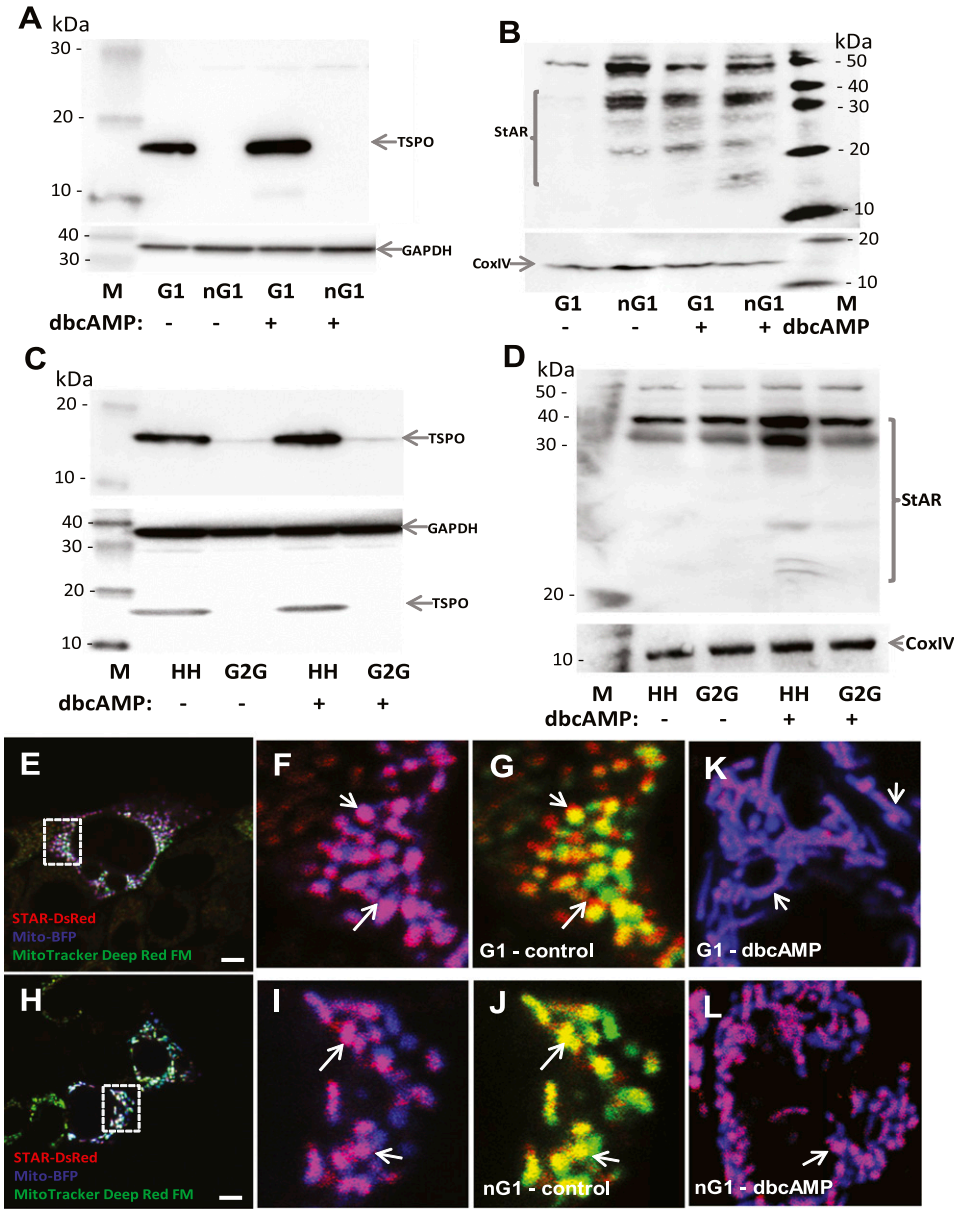

Figure 7. TSPO is involved in the function and/or mitochondrial import of STAR. (A, C) Immunoblot analyses for TSPO in cell lysates from controls (G1 and HH cells) and TSPO-deficient cells (nG1 and G2G) treated with and without dbcAMP (1 mM) for 2 hours. Robust TSPO expression is seen in G1 and HH cells. No TSPO expression is seen in nG1 cells; weak TSPO expression is seen in G2G cells. (B, D) Immunoblot analyses of STAR in lysates from controls (G1 and HH cells) and TSPO-deficient cells (nG1 and G2G) treated with and without dbcAMP (1 mM) for 2 hours. Immunoreactive STAR proteins were induced by depletion of TSPO in nG1 cells. Anti–glyceraldehyde-3-phosphate dehydrogenase (36 kDa) was used for reprobing the same membrane used for TSPO, whereas anti-Cox IV (16 kDa) was used to reprobe the same membrane used for anti-STAR. The gel photos were taken using the Bio-Rad Gel Imager. (E–J) Confocal images of the STAR-DsRed fusion protein used for validation of the STAR protein mitochondrial import. Insets in panel (E) identify the areas shown in (F) and (G), and insets in panel (H) identify the areas shown in panels (I) and (J). STAR-DsRed protein is (G) localized remarkably outside the mitochondria in control G1 cells but (J) localized more within the mitochondria and less outside the mitochondria in nG1 TSPO-deficient cells, in comparison with mitochondria-targeted blue fluorescent protein and Mitotracker Deep Red Fm staining. (K) After 1-mM dbcAMP treatment, the STAR-DsRed was imported into the mitochondria in control G1 cells; (L) however, a still remarkable amount of the protein stayed outside the mitochondria in the mutant nG1 cells. The STAR mitochondrial import may be correlated with the $\Delta\psi_m$ (45, 46). White arrows indicate the distribution of STAR-DsRed fusion protein (red) (F, G, I and J) on the surface or (K) inside mitochondria. Scale bar: 5 μm. M, protein ladder.

Discussion

Data from several independent laboratories have shown an important role of TSPO in steroidogenesis (10, 23, 25, 47–51). In addition to the stimulatory effect of numerous TSPO-specific drug ligands on steroid production both *in vivo* and *in vitro*, in all steroidogenic cells and tissues tested, the role of TSPO in steroidogenesis is supported strongly by studies of the effects of the specific inhibition of TSPO-specific ligands on steroid formation (5, 52). In particular, several TSPO ligands that bind either to the drug-binding sites or to the cholesterol

recognition/interaction amino acid consensus domains of TSPO were shown to block hormone-induced steroid formation in cells both *in vitro* and *in vivo*. These ligands include flunitrazepam, 5-androsten-3β,17,19-triol, imidazo[1,2-a]pyridine–containing and triazol-containing ligands, and peptide antagonists identified through a phage library screening (53–57).

However, recent studies in rodents with genetic depletion of TSPO reported results inconsistent with those of many studies reporting a critical role for TSPO in steroid formation (20, 22, 23, 58–60). In the first study of the genetic depletion of TSPO in a mouse model by *Amhr2*-Cre–mediated *Tspo* conditional knockout (cKO), the authors concluded that TSPO is not required for steroid biosynthesis (20). However, although the *Amhr2*-Cre–mediated *Tspo* cKO approach had been used for the KO of other genes, the early expression of the *Amhr2* gene during preimplantation stages of mouse development could lead to a gene's global KO and/or WT-like animals with a cKO genotype and thus to an animal population with mixed variable genotypes (22). Using CRISPR/Cas9 technology to knock out *Tspo* in MA-10 cells, the same group of investigators again argued against an intimate relationship between TSPO and steroidogenesis and argued that the effect of the high-affinity TSPO ligand PK 11195 on steroid formation is independent of TSPO (26). If validated, these results would challenge the use of PK 11195 as a diagnostic ligand for the TSPO protein (31, 61). These findings clearly argue for further investigation using the MA-10 system to clarify and extend our understanding of the relationship between TSPO and steroidogenesis.

To this end, we used the CRISPR/Cas9 system to create *Tspo*-specific mutations in MA-10 cells and then examined the effects on steroid formation. Two mutant subcell lines were developed, each carrying a *Tspo* exon2–specific genome modification. Similar levels of basal progesterone were seen between the control and *Tspo* mutant cells. These observations suggest that CYP11A1 and HSD3B1, the enzymes responsible for cholesterol metabolism downstream of TSPO, were functionally intact. Indeed, CYP11A1 expression levels in TSPO-deficient cells were found to be the same as in WT cells. Importantly, in response to dbcAMP, both *Tspo* mutant cell lines exhibited reduced progesterone formation in comparison with the corresponding control cells, but with different features in terms of the reduction in progesterone production, which are most likely due to cell line–specific mitochondrial redox conditions (28). These results support the long-held contention of an important role for TSPO in steroid formation. Moreover, we found a buildup of LDs in the cytosol of the mutant cells, suggesting a deficiency in the ability of the cells to translocate lipid into the mitochondria. In addition, we observed that *Tspo* mutant cells lost the ability to respond to the TSPO drug ligand PK 11195 to produce progesterone, unlike control cells. These findings strongly support an important role of TSPO in steroidogenesis, in contrast to previous negative reports (20, 26). The discrepant results are most likely due to the different systems used or the different approaches taken in the interpretation of the results.

The current study provides strong evidence of a role for TSPO in regulation of $\Delta\psi_m$ in MA-10 cell mitochondria. Among the experimental approaches and studies that lead to this conclusion are $\Delta\psi_m$-dependent MitoTracker staining with a pattern of predominantly peripheral distribution in mitochondria; OMM morphology; TEM studies of the contact sites between the OMM and the IMM; JC-10 staining indicating a decrease in the red/green fluorescence intensity ratio; the effects of TSPO-specific ligands (PK 11195 and XBD173) on the repolarization of mitochondria; and the association of $\Delta\psi_m$ with mitochondrial redox homeostasis. However, change in $\Delta\psi_m$ in MA-10 cells under TSPO deficiency behaves in a reversible manner because PKA inhibition hyperpolarizes the mitochondria, whereas dbcAMP-stimulated PKA activation decreases $\Delta\psi_m$. These observations are consistent with the report that cAMP stimulation decreases $\Delta\psi_m$ but that cAMP inhibition repolarizes the mitochondria (39).

The $\Delta\Psi_M$ of the mutant cells was significantly reduced compared with that of control cells. This finding is in agreement with a previous report showing a decreased $\Delta\psi_m$ in fibroblast mitochondria in response to TSPO deficiency (62). These findings suggest a possible role for TSPO in the regulation of $\Delta\psi_m$ and thus in maintaining normal mitochondrial function. $\Delta\psi_m$ reflects mitochondrial function in the maintenance of the respiratory chain, generation of adenosine triphosphate, cellular differentiation, and apoptosis. With regard to apoptosis, the lower the $\Delta\psi_m$, the more susceptible cells are to apoptotic stimuli (63). However, our results show that the reduced $\Delta\psi_m$ in TSPO-deficient cells neither affected cell proliferation nor increased apoptosis in response to dbcAMP treatment. In contrast, *Tspo* deletion led to resistance to apoptosis. This finding is in agreement with previous reports on the *Drosophila* TSPO ortholog (CG2789/dTSPO) (64) and on the antiapoptotic effects of TSPO-specific ligands (*e.g.,* PK 11195) and *Tspo* knockdown (65, 66). These results suggest that reduced steroid production by *Tspo* mutant cells was not due to apoptotic cell death after dbcAMP treatment. It should be noted that TSPO has been thought to regulate $\Delta\psi_m$ *via* its interaction with the mitochondrial membrane permeability transition pore, though this is not without controversy (65, 67, 68).

Reduction in $\Delta\Psi_M$ of the *Tspo* mutant cells is most likely attributable to TSPO interactions with the VDAC and tubulin (dimeric and polymerized) at the OMM (Supplemental Fig. 7). This conclusion is based on findings using the tubulin stabilizing reagent paclitaxel (Sigma-Aldrich Canada Ltd.) showing that TSPO interfered with a membrane lipid composition–dependent VDAC/tubulin interaction (39, 69). Paclitaxel has been shown to bind the interior surface of microtubules (70), and tubulin has been reported to interact with VDAC1 in regulation of mitochondrial respiration as well as $\Delta\psi_m$ (40, 41). The $\Delta\psi_m$ depends on the flux of respiratory substrates adenosine triphosphate, adenosine diphosphate, and Pi through the VDAC, whereas the VDAC is controlled by tubulin. Adenine nucleotide translocator also plays a role in maintenance of the $\Delta\psi_m$ (39, 71). Therefore, TSPO apparently controls cellular and mitochondrial metabolism in MA-10 cells in general *via* regulation of $\Delta\psi_m$, and affects OMM permeability and/or outer and inner membrane contacts/fusion, as hypothesized previously (72). This suggests that the contact sites are essential for dbcAMP-stimulated steroidogenesis. The changes in mitochondrial membranes may be related to TSPO-mediated membrane properties, such as their dynamics, physical properties, and facilitating or impairing of mitochondrial membrane permeabilization with dbcAMP treatment. Indeed, the $\Delta\psi_m$ is needed for mitochondrial fusion, which in turn is required for steroid biosynthesis (34).

STAR, another protein known to be integrally involved in steroid formation, was induced in nG1 cells, suggesting the possible involvement of TSPO in STAR functioning/mitochondrial import. Thus, the $\Delta\psi_m$ is necessary for STAR protein mitochondrial import in Leydig cells in steroidogenesis (45, 73). Our immunoblot analysis and confocal imaging results are consistent with the concept that the STAR protein works on the mitochondrial surface rather than inside the mitochondria (74). However, whether STAR is inside mitochondria (nG1 cells) or outside mitochondria (G2G cells), it acts functionally with TSPO, an OMM protein, during hormone-stimulated steroidogenesis. How STAR functions in relationship to TSPO to deliver cholesterol into the mitochondria remains to be elucidated (72). Nevertheless, these observations are in agreement with previous findings that TSPO is involved in STAR import into mitochondria and processing either directly or indirectly via changes in $\Delta\psi_m$ (24, 53, 75).

Taken together, these results provide further compelling evidence for a critical role of TSPO in steroid biosynthesis and suggest that it may function at least in part *via* its regulation of $\Delta\Psi_m$ and effects on STAR synthesis and/or processing.

Acknowledgments

We thank Dr. Mario Ascoli (University of Iowa, Iowa City, IA) for supplying the MA-10 cell line, and Ms. Jeannie Mui for performing the TEM at the Facility for Electron Microscopy Research, McGill University. We also thank the Immunophenotyping and Molecular Imaging Platforms of the Research Institute of the McGill University Health Centre.

Financial Support: This work was supported by Canadian Institutes of Health Research Grants MOP125983 and PJT148659 (to V.P.), a Canada Research Chair in Biochemical Pharmacology (to V.P.), the John Stauffer Dean's Chair in Pharmaceutical Sciences (University of Southern California; to V.P.), and National Institutes of Health Grants R37 AG021092 and R21 AG051259 (to B.Z.).

Correspondence: Vassilios Papadopoulos, PhD, Department of Pharmacology and Pharmaceutical Sciences, School of Pharmacy, University of Southern California, Los Angeles, California 90089. E-mail: vpapadop@usc.edu.

Disclosure Summary: The authors have nothing to disclose.

References

1. Kraemer FB, Shen WJ, Azhar S. SNAREs and cholesterol movement for steroidogenesis. *Mol Cell Endocrinol*. 2017;**441**:17–21.
2. Fan J, Papadopoulos V. Evolutionary origin of the mitochondrial cholesterol transport machinery reveals a universal mechanism of steroid hormone biosynthesis in animals. *PLoS One*. 2013;**8**(10):e76701.
3. Stocco DM, Zhao AH, Tu LN, Morohaku K, Selvaraj V. A brief history of the search for the protein(s) involved in the acute regulation of steroidogenesis. *Mol Cell Endocrinol*. 2017;**441**:7–16.
4. Shen WJ, Azhar S, Kraemer FB. Lipid droplets and steroidogenic cells. *Exp Cell Res*. 2016;**340**(2):209–214.
5. Papadopoulos V, Aghazadeh Y, Fan J, Campioli E, Zirkin B, Midzak A. Translocator protein-mediated pharmacology of cholesterol transport and steroidogenesis. *Mol Cell Endocrinol*. 2015;**408**:90–98.
6. Miller WL. Mechanism of StAR's regulation of mitochondrial cholesterol import. *Mol Cell Endocrinol*. 2007;**265-266**:46–50.
7. Issop L, Fan J, Lee S, Rone MB, Basu K, Mui J, Papadopoulos V. Mitochondria-associated membrane formation in hormone-stimulated Leydig cell steroidogenesis: role of ATAD3. *Endocrinology*. 2015;**156**(1):334–345.
8. Lin Y, Hou X, Shen WJ, Hanssen R, Khor VK, Cortez Y, Roseman AN, Azhar S, Kraemer FB. SNARE-mediated cholesterol movement to mitochondria supports steroidogenesis in rodent cells. *Mol Endocrinol*. 2016;**30**(2):234–247.
9. Arakane F, Kallen CB, Watari H, Stayrook SE, Lewis M, Strauss JF III. Steroidogenic acute regulatory protein (StAR) acts on the outside of mitochondria to stimulate steroidogenesis. *Endocr Res*. 1998;**24**(3-4):463–468.
10. Papadopoulos V, Baraldi M, Guilarte TR, Knudsen TB, Lacapère JJ, Lindemann P, Norenberg MD, Nutt D, Weizman A, Zhang MR, Gavish M. Translocator protein (18kDa): new nomenclature for the peripheral-type benzodiazepine receptor based on its structure and molecular function. *Trends Pharmacol Sci*. 2006;**27**(8):402–409.
11. Rone MB, Midzak AS, Issop L, Rammouz G, Jagannathan S, Fan J, Ye X, Blonder J, Veenstra T, Papadopoulos V. Identification of a dynamic mitochondrial protein complex driving cholesterol import, trafficking, and metabolism to steroid hormones. *Mol Endocrinol*. 2012;**26**(11):1868–1882.
12. Li H, Papadopoulos V. Peripheral-type benzodiazepine receptor function in cholesterol transport: identification of a putative

cholesterol recognition/interaction amino acid sequence and consensus pattern. *Endocrinology*. 1998;**139**(12):4991–4997.
13. Jamin N, Neumann JM, Ostuni MA, Vu TK, Yao ZX, Murail S, Robert JC, Giatzakis C, Papadopoulos V, Lacapère JJ. Characterization of the cholesterol recognition amino acid consensus sequence of the peripheral-type benzodiazepine receptor. *Mol Endocrinol*. 2005;**19**(3):588–594.
14. Li F, Liu J, Zheng Y, Garavito RM, Ferguson-Miller S. Crystal structures of translocator protein (TSPO) and mutant mimic of a human polymorphism. *Science*. 2015;**347**(6221):555–558.
15. Aghazadeh Y, Zirkin BR, Papadopoulos V. Pharmacological regulation of the cholesterol transport machinery in steroidogenic cells of the testis. *Vitam Horm*. 2015;**98**:189–227.
16. Midzak A, Zirkin B, Papadopoulos V. Translocator protein: pharmacology and steroidogenesis. *Biochem Soc Trans*. 2015;**43**(4):572–578.
17. Elustondo P, Martin LA, Karten B. Mitochondrial cholesterol import. *Biochim Biophys Acta*. 2017;**1862**(1):90–101.
18. Rone MB, Fan J, Papadopoulos V. Cholesterol transport in steroid biosynthesis: role of protein-protein interactions and implications in disease states. *Biochim Biophys Acta*. 2009;**1791**(7):646–658.
19. Marí M, Morales A, Colell A, García-Ruiz C, Fernández-Checa JC. Mitochondrial glutathione, a key survival antioxidant. *Antioxid Redox Signal*. 2009;**11**(11):2685–2700.
20. Morohaku K, Pelton SH, Daugherty DJ, Butler WR, Deng W, Selvaraj V. Translocator protein/peripheral benzodiazepine receptor is not required for steroid hormone biosynthesis. *Endocrinology*. 2014;**155**(1):89–97.
21. Tu LN, Morohaku K, Manna PR, Pelton SH, Butler WR, Stocco DM, Selvaraj V. Peripheral benzodiazepine receptor/translocator protein global knock-out mice are viable with no effects on steroid hormone biosynthesis. *J Biol Chem*. 2014;**289**(40):27444–27454.
22. Fan J, Campioli E, Midzak A, Culty M, Papadopoulos V. Conditional steroidogenic cell-targeted deletion of TSPO unveils a crucial role in viability and hormone-dependent steroid formation. *Proc Natl Acad Sci USA*. 2015;**112**(23):7261–7266.
23. Papadopoulos V, Fan J, Zirkin B. Translocator protein (18 kDa): an update on its function in steroidogenesis [published online ahead of print July 1, 2017]. *J Neuroendocrinol*. doi: 10.1111/jne.12500.
24. Hauet T, Yao ZX, Bose HS, Wall CT, Han Z, Li W, Hales DB, Miller WL, Culty M, Papadopoulos V. Peripheral-type benzodiazepine receptor-mediated action of steroidogenic acute regulatory protein on cholesterol entry into Leydig cell mitochondria. *Mol Endocrinol*. 2005;**19**(2):540–554.
25. Kelly-Hershkovitz E, Weizman R, Spanier I, Leschiner S, Lahav M, Weisinger G, Gavish M. Effects of peripheral-type benzodiazepine receptor antisense knockout on MA-10 Leydig cell proliferation and steroidogenesis. *J Biol Chem*. 1998;**273**(10):5478–5483.
26. Tu LN, Zhao AH, Stocco DM, Selvaraj V. PK11195 effect on steroidogenesis is not mediated through the translocator protein (TSPO). *Endocrinology*. 2015;**156**(3):1033–1039.
27. Ascoli M. Characterization of several clonal lines of cultured Leydig tumor cells: gonadotropin receptors and steroidogenic responses. *Endocrinology*. 1981;**108**(1):88–95.
28. Fan J, Li X, Issop L, Culty M, Papadopoulos V. ACBD2/ECI2-mediated peroxisome-mitochondria interactions in Leydig cell steroid biosynthesis. *Mol Endocrinol*. 2016;**30**(7):763–782.
29. Fan J, Rone MB, Papadopoulos V. Translocator protein 2 is involved in cholesterol redistribution during erythropoiesis. *J Biol Chem*. 2009;**284**(44):30484–30497.
30. Spyropoulos IC, Liakopoulos TD, Bagos PG, Hamodrakas SJ. TMRPres2D: high quality visual representation of transmembrane protein models. *Bioinformatics*. 2004;**20**(17):3258–3260.
31. Jaremko M, Jaremko Ł, Jaipuria G, Becker S, Zweckstetter M. Structure of the mammalian TSPO/PBR protein. *Biochem Soc Trans*. 2015;**43**(4):566–571.
32. Guex N, Peitsch MC. SWISS-MODEL and the Swiss-PdbViewer: an environment for comparative protein modeling. *Electrophoresis*. 1997;**18**(15):2714–2723.
33. Khor VK, Ahrends R, Lin Y, Shen WJ, Adams CM, Roseman AN, Cortez Y, Teruel MN, Azhar S, Kraemer FB. The proteome of cholesteryl-ester-enriched versus triacylglycerol-enriched lipid droplets. *PLoS One*. 2014;**9**(8):e105047.
34. Duarte A, Poderoso C, Cooke M, Soria G, Cornejo Maciel F, Gottifredi V, Podestá EJ. Mitochondrial fusion is essential for steroid biosynthesis. *PLoS One*. 2012;**7**(9):e45829.
35. Hanson GT, Aggeler R, Oglesbee D, Cannon M, Capaldi RA, Tsien RY, Remington SJ. Investigating mitochondrial redox potential with redox-sensitive green fluorescent protein indicators. *J Biol Chem*. 2004;**279**(13):13044–13053.
36. Reers M, Smiley ST, Mottola-Hartshorn C, Chen A, Lin M, Chen LB. Mitochondrial membrane potential monitored by JC-1 dye. *Methods Enzymol*. 1995;**260**:406–417.
37. Sirenko O, Hesley J, Rusyn I, Cromwell EF. High-content assays for hepatotoxicity using induced pluripotent stem cell-derived cells. *Assay Drug Dev Technol*. 2014;**12**(1):43–54.
38. Li W, Yang C, Lu J, Huang P, Barnstable CJ, Zhang C, Zhang SS. Tetrandrine protects mouse retinal ganglion cells from ischemic injury. *Drug Des Devel Ther*. 2014;**8**:327–339.
39. Maldonado EN, Patnaik J, Mullins MR, Lemasters JJ. Free tubulin modulates mitochondrial membrane potential in cancer cells. *Cancer Res*. 2010;**70**(24):10192–10201.
40. Rostovtseva TK, Sheldon KL, Hassanzadeh E, Monge C, Saks V, Bezrukov SM, Sackett DL. Tubulin binding blocks mitochondrial voltage-dependent anion channel and regulates respiration. *Proc Natl Acad Sci USA*. 2008;**105**(48):18746–18751.
41. Rostovtseva TK, Bezrukov SM. VDAC inhibition by tubulin and its physiological implications. *Biochim Biophys Acta*. 2012;**1818**(6):1526–1535.
42. Clark MA, Shay JW. The role of tubulin in the steroidogenic response of murine adrenal and rat Leydig cells. *Endocrinology*. 1981;**109**(6):2261–2263.
43. Gatliff J, East D, Crosby J, Abeti R, Harvey R, Craigen W, Parker P, Campanella M. TSPO interacts with VDAC1 and triggers a ROS-mediated inhibition of mitochondrial quality control [published correction appears in *Autophagy*. 2016;12(2):4420]. *Autophagy*. 2014;**10**(12):2279–2296.
44. Granot Z, Kobiler O, Melamed-Book N, Eimerl S, Bahat A, Lu B, Braun S, Maurizi MR, Suzuki CK, Oppenheim AB, Orly J. Turnover of mitochondrial steroidogenic acute regulatory (StAR) protein by Lon protease: the unexpected effect of proteasome inhibitors. *Mol Endocrinol*. 2007;**21**(9):2164–2177.
45. King SR, Liu Z, Soh J, Eimerl S, Orly J, Stocco DM. Effects of disruption of the mitochondrial electrochemical gradient on steroidogenesis and the Steroidogenic Acute Regulatory (StAR) protein. *J Steroid Biochem Mol Biol*. 1999;**69**(1-6):143–154.
46. Martin J, Mahlke K, Pfanner N. Role of an energized inner membrane in mitochondrial protein import: delta psi drives the movement of presequences. *J Biol Chem*. 1991;**266**(27):18051–18057.
47. Papadopoulos V. On the role of the translocator protein (18-kDa) TSPO in steroid hormone biosynthesis. *Endocrinology*. 2014;**155**(1):15–20.
48. Papadopoulos V, Mukhin AG, Costa E, Krueger KE. The peripheral-type benzodiazepine receptor is functionally linked to Leydig cell steroidogenesis. *J Biol Chem*. 1990;**265**(7):3772–3779.
49. Mukhin AG, Papadopoulos V, Costa E, Krueger KE. Mitochondrial benzodiazepine receptors regulate steroid biosynthesis. *Proc Natl Acad Sci USA*. 1989;**86**(24):9813–9816.
50. Krueger KE, Papadopoulos V. Peripheral-type benzodiazepine receptors mediate translocation of cholesterol from outer to inner mitochondrial membranes in adrenocortical cells. *J Biol Chem*. 1990;**265**(25):15015–15022.
51. Gavish M, Weizman R. Role of peripheral-type benzodiazepine receptors in steroidogenesis. *Clin Neuropharmacol*. 1997;**20**(6):473–481.
52. Lacapère JJ, Papadopoulos V. Peripheral-type benzodiazepine receptor: structure and function of a cholesterol-binding protein in steroid and bile acid biosynthesis. *Steroids*. 2003;**68**(7-8):569–585.

53. Gazouli M, Han Z, Papadopoulos V. Identification of a peptide antagonist to the peripheral-type benzodiazepine receptor that inhibits hormone-stimulated Leydig cell steroid formation. *J Pharmacol Exp Ther*. 2002;**303**(2):627–632.
54. Midzak A, Akula N, Lecanu L, Papadopoulos V. Novel androstenetriol interacts with the mitochondrial translocator protein and controls steroidogenesis. *J Biol Chem*. 2011;**286**(11):9875–9887.
55. Midzak A, Denora N, Laquintana V, Cutrignelli A, Lopedota A, Franco M, Altomare CD, Papadopoulos V. 2-Phenylimidazo[1,2-a]pyridine-containing ligands of the 18-kDa translocator protein (TSPO) behave as agonists and antagonists of steroidogenesis in a mouse leydig tumor cell line. *Eur J Pharm Sci*. 2015;**76**:231–237.
56. Midzak AS, Akula N, Rone MB, Papadopoulos V. Computational modeling and biological validation of novel non-steroidal ligands for the cholesterol recognition/interaction amino acid consensus (CRAC) motif of the mitochondrial translocator protein (TSPO). *Pharmacol Res*. 2015;**99**:393–403.
57. Papadopoulos V, Nowzari FB, Krueger KE. Hormone-stimulated steroidogenesis is coupled to mitochondrial benzodiazepine receptors: tropic hormone action on steroid biosynthesis is inhibited by flunitrazepam. *J Biol Chem*. 1991;**266**(6):3682–3687.
58. Owen DR, Fan J, Campioli E, Venugopal S, Midzak A, Daly E, Harlay A, Issop L, Libri V, Kalogiannopoulou D, Oliver E, Gallego-Colon E, Colasanti A, Huson L, Rabiner EA, Suppiah P, Essagian C, Matthews PM, Papadopoulos V. TSPO mutations in rats and a human polymorphism impair the rate of steroid synthesis. *Biochem J*. 2017;**474**(23):3985–3999.
59. Banati RB, Middleton RJ, Chan R, Hatty CR, Kam WW, Quin C, Graeber MB, Parmar A, Zahra D, Callaghan P, Fok S, Howell NR, Gregoire M, Szabo A, Pham T, Davis E, Liu GJ. Positron emission tomography and functional characterization of a complete PBR/TSPO knockout. *Nat Commun*. 2014;**5**:5452.
60. Barron AM, Ji B, Kito S, Suhara T, Higuchi M. Steroidogenic abnormalities in translocator protein knockout mice and significance in the aging male. *Biochem J*. 2017;BCJ20170645.
61. Rupprecht R, Papadopoulos V, Rammes G, Baghai TC, Fan J, Akula N, Groyer G, Adams D, Schumacher M. Translocator protein (18 kDa) (TSPO) as a therapeutic target for neurological and psychiatric disorders. *Nat Rev Drug Discov*. 2010;**9**(12):971–988.
62. Zhao AH, Tu LN, Mukai C, Sirivelu MP, Pillai VV, Morohaku K, Cohen R, Selvaraj V. Mitochondrial translocator protein (TSPO) function is not essential for heme biosynthesis. *J Biol Chem*. 2016;**291**(4):1591–1603.
63. Zhang BB, Wang DG, Guo FF, Xuan C. Mitochondrial membrane potential and reactive oxygen species in cancer stem cells. *Fam Cancer*. 2015;**14**(1):19–23.
64. Lin R, Angelin A, Da Settimo F, Martini C, Taliani S, Zhu S, Wallace DC. Genetic analysis of dTSPO, an outer mitochondrial membrane protein, reveals its functions in apoptosis, longevity, and Ab42-induced neurodegeneration. *Aging Cell*. 2014;**13**(3):507–518.
65. Veenman L, Gavish M. The role of 18 kDa mitochondrial translocator protein (TSPO) in programmed cell death, and effects of steroids on TSPO expression. *Curr Mol Med*. 2012;**12**(4):398–412.
66. Zeno S, Zaaroor M, Leschiner S, Veenman L, Gavish M. CoCl(2) induces apoptosis via the 18 kDa translocator protein in U118MG human glioblastoma cells. *Biochemistry*. 2009;**48**(21):4652–4661.
67. Šileikytė J, Blachly-Dyson E, Sewell R, Carpi A, Menabò R, Di Lisa F, Ricchelli F, Bernardi P, Forte M. Regulation of the mitochondrial permeability transition pore by the outer membrane does not involve the peripheral benzodiazepine receptor (Translocator Protein of 18 kDa (TSPO)). *J Biol Chem*. 2014;**289**(20):13769–13781.
68. Šileikytė J, Petronilli V, Zulian A, Dabbeni-Sala F, Tognon G, Nikolov P, Bernardi P, Ricchelli F. Regulation of the inner membrane mitochondrial permeability transition by the outer membrane translocator protein (peripheral benzodiazepine receptor). *J Biol Chem*. 2011;**286**(2):1046–1053.
69. Rostovtseva TK, Gurnev PA, Chen MY, Bezrukov SM. Membrane lipid composition regulates tubulin interaction with mitochondrial voltage-dependent anion channel. *J Biol Chem*. 2012;**287**(35):29589–29598.
70. Dumontet C, Jordan MA. Microtubule-binding agents: a dynamic field of cancer therapeutics. *Nat Rev Drug Discov*. 2010;**9**(10):790–803.
71. Liu Y, Chen XJ. Adenine nucleotide translocase, mitochondrial stress, and degenerative cell death. *Oxid Med Cell Longev*. *2013*;**2013**:146860.
72. Thomson M. Does cholesterol use the mitochondrial contact site as a conduit to the steroidogenic pathway? *BioEssays*. 2003;**25**(3):252–258.
73. Allen JA, Shankara T, Janus P, Buck S, Diemer T, Hales KH, Hales DB. Energized, polarized, and actively respiring mitochondria are required for acute Leydig cell steroidogenesis. *Endocrinology*. 2006;**147**(8):3924–3935.
74. Arakane F, Sugawara T, Nishino H, Liu Z, Holt JA, Pain D, Stocco DM, Miller WL, Strauss JF III. Steroidogenic acute regulatory protein (StAR) retains activity in the absence of its mitochondrial import sequence: implications for the mechanism of StAR action. *Proc Natl Acad Sci USA*. 1996;**93**(24):13731–13736.
75. Estabrook RW, Rainey WE. Twinkle, twinkle little StAR, how we wonder what you are. *Proc Natl Acad Sci USA*. 1996;**93**(24):13552–13554.